Numerical Simulations of Gold-Coated Aluminum Foils Heated by the KALIF Applied-B Diode Proton Beam

J.J. MacFarlane, P. Wang, D.H. Cohen

December 1997

UWFDM-1060

FUSION TECHNOLOGY INSTITUTE

UNIVERSITY OF WISCONSIN

MADISON WISCONSIN

Numerical Simulations of Gold-Coated Aluminum Foils Heated by the KALIF Applied-B Diode Proton Beam

J. J. MacFarlane, P. Wang, and D. H. Cohen

Fusion Technology Institute
University of Wisconsin-Madison
1500 Engineering Drive
Madison, WI 53706

December 1997

UWFDM-1060

Contents

1. Introduction

The purpose of this report is to describe theoretical and computational work performed during the 1997 calendar year in support of the Forschungszentrum Karlsruhe (FZK) KALIF program. This work, summarized in Table 1.1, has been concentrated primarily in three areas. First, we have performed atomic physics calculations using ATBASE [1] for computing the K_α spectra for elements magnesium (Mg), silicon (Si), and phosphorous (P). These data tables were supplied to FZK scientists in April 1997. Second, because we have made a large number of improvements to our collisional-radiative code NLTERT since the first writing of the NLTERT User's Guide in December 1993, we have updated the user's guide and provided copies of it to FZK in September 1997 [2]. Finally, prompted by discussions with FZK scientists, we have performed simulations for potential two-foil targets which could be used in future KALIF experiments. These targets consisted of a 6 μm-thick aluminum foil, backed by a gold foil of varying thickness (0.1 μm to 10 μm). The gold foil was positioned such that the proton beam passes through the gold prior to entering the Al layer. The purpose of our modeling was to assess the effects of the gold layer on the heating of the Al layer, as well as compute its effect on the K_α line emission from the Al layer.

Also during 1997, we participated in the 8th International Workshop on Atomic Physics for Ion-Driven Fusion at Heidelberg, Germany in September 1997. Here, we presented a paper on "The Influence of Energetic Particles on the Spectral Properties and Ionization Dynamics of Plasmas Heated by Intense Light Ion Beams." At this workshop, we also discussed with KALIF scientists our progress on work supported by FZK. Finally, a paper related to our KALIF work, "Diagnosing Plasma Conditions in Targets Irradiated by Intense Light Ion Beams Using K_α Satellite Line Intensity Ratios," [3] was submitted for publication.

Table 1.1. Tasks for 1997

1. Perform collisional-radiative equilibrium (CRE) and atomic physics calculations in support of KALIF beam-plasma interaction experiments, particularly the K_α spectra of Mg, Si, and P.
   (a) Analyze K_α satellite emission and/or absorption spectral data obtained in KALIF experiments;
   (b) Perform calculations to set up atomic physics databases and identify K_α lines observed in KALIF experiments;
   (c) Using temperature and density distributions from radiation-hydrodynamics simulations, compute synthetic time-dependent and time-integrated spectra for KALIF experiments.
2. Update NLTERT User's Guide to include code modifications between December 1993 and 1997.
3. Document results in Final Report to FZK. Supply FZK with updated NLTERT and ATBASE codes.

2. Simulation of Proton Beam-Heated Gold/Aluminum Targets

In this section, we present results from radiation-hydrodynamics and collisional-radiative calculations for gold/aluminum (Au/Al) targets heated by an intense proton beam. Beam parameters are taken to be those typical of KALIF experiments in which an applied-B diode is used. The thickness of the Al is 6 μm in all simulations. The Au layer, which is attached to the Al and located on the side facing the incident proton beam, has a thickness ranging from 0.1 μm to 10 μm. The goal is to predict the sensitivity of the time-dependent heating of the Al layer and the resulting K_α satellite line spectrum to the thickness of the gold layer. One should expect some sensitivity because a gold layer can reduce the beam voltage (that is, the proton kinetic energy) in the Al, which in turn increases the stopping power and heating rate. Therefore, one could expect the Al K_α spectrum to exhibit stronger emission from the satellites of relatively high ionization stages. On the other hand, a reduction in the voltage also leads to a lower proton-impact ionization cross section for K-shell electrons of the target ions. This reduces the overall K_α photon flux at the spectrometer. The purpose of the calculations discussed below is to make quantitative predictions for these effects, and provide insights for potential future KALIF experiments.

2.1. Proton Beam Parameters and Target Geometry

Figure 2.1 shows the time-dependent beam voltage, current density, and power density used in these simulations. It also shows a schematic illustration of the beam-target geometry. The spatial dependence of the beam current density across the target is modeled as a Gaussian distribution:

$$f(r) = \frac{1}{\pi R_0^2}\, e^{-(r/R_0)^2}\,, \tag{2.1}$$

where r is the distance from the center of the beam (i.e., the middle of circle A in Figure 2.1, and $R_0 = 0.37$ cm, which corresponds to a FWHM of 0.62 cm). Because our radiation-hydrodynamics simulations are performed using a 1-D code [4], with the position dependence provided in the direction of beam propagation, we have divided the target into four "regions", labelled A, B, C, and D (Region A being the "hottest"). Separate 1-D radiation-hydrodynamics and collisional-radiative equilibrium (CRE) calculations are performed for each region.

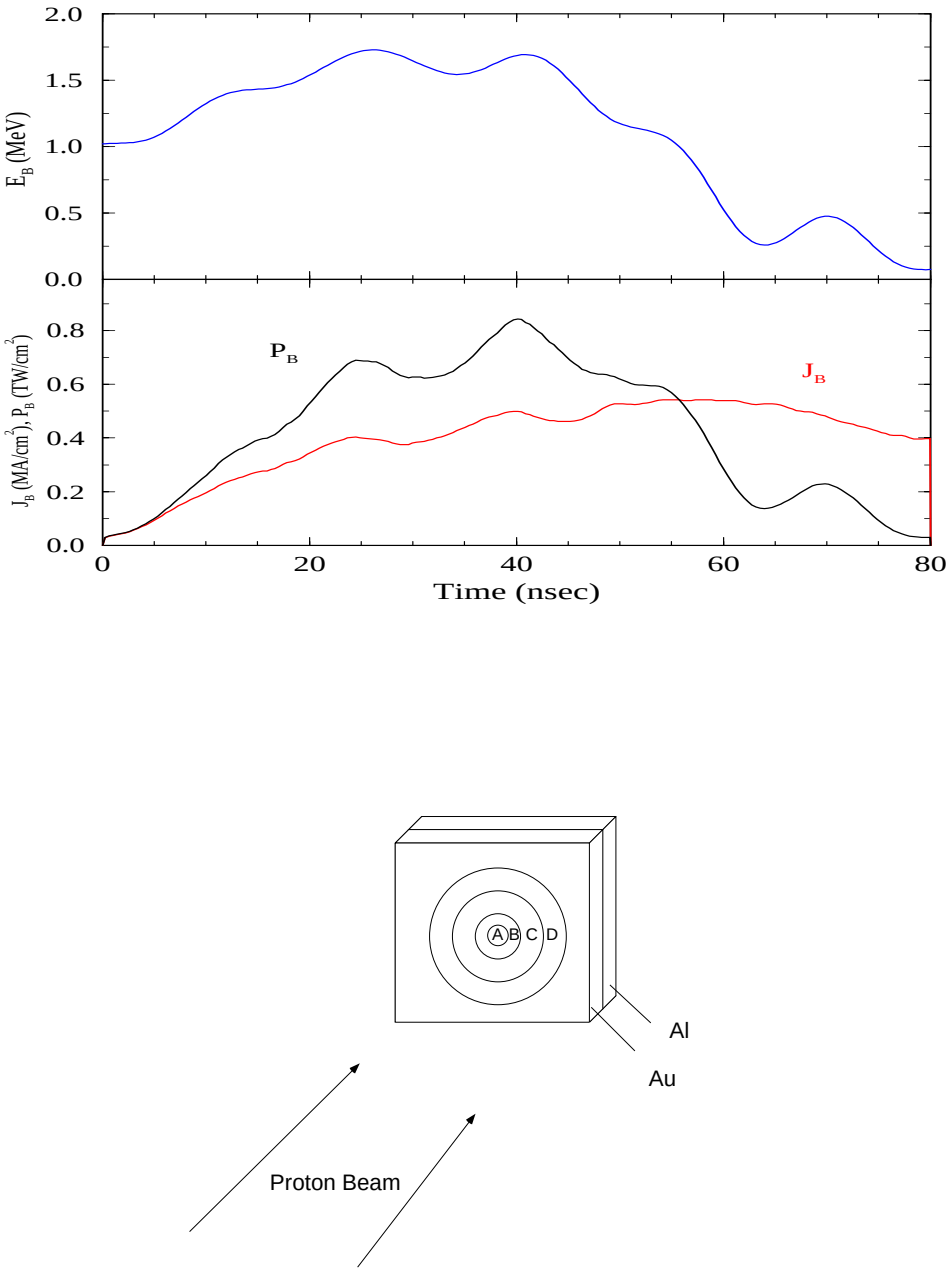

Figure 2.1. Top: Time-dependent beam voltage, current density, and power density used in K_α target simulations. The current density shown corresponds to the peak value at the center of the beam, $J_{\rm peak}(t)$. Bottom: Schematic illustration of the beam-target geometry.

The current and power densities in Figure 2.1 correspond to the values at the *peak* of the spatial Gaussian profile. For each simulation region, the peak current density is multiplied by a constant to reflect the change across the Gaussian profile. After performing CRE calculations to get the K_α satellite spectra for each region, we perform a space-integration of the results using areal weights which reflect the assumed beam geometry. Table 2.1 shows for each region the outer radius of the region (r/R_0), the area of the region ($A/\pi R_0^2$), the current density multiplier (J/J_{peak}), and the fraction of the total beam current entering each region (I/I_{tot}). For all cases, the time-dependent beam voltage is that shown in Figure 2.1.

Additional discussion regarding modeling of the space- and time-dependent beam parameters is given in References [5] and [6].

Table 2.1. Region-Dependent Beam Conditions on Target Plane

Region	r/R_0	$I/I_{\rm tot}$	$A/\pi R_0^2$	$J/J_{\rm peak}$
A	0.5	0.221	0.250	0.884
B	0.8	0.252	0.390	0.646
C	1.2	0.290	0.800	0.363
D	2.0	0.219	2.56	0.086

2.2. Results from Radiation-Hydrodynamics Simulations

Simulations were performed for Au/Al targets using the BUCKY 1-D radiation-hydrodynamics code. To assess the effects of the Au foil thickness on the time-dependent heating of the Al layer, we performed a series of calculations for Au foils ranging in thickness from 0.1 μm to 10 μm using the beam parameters shown in Figure 2.1 ($J(t)/J_{peak} = 1$). In all cases, the Al foil thickness was 6 μm (1.62 mg/cm^2).

Results for the average temperature (mass-weighted average over Lagrangian zones) are shown as a function of time for the Al and Au layers in Figures 2.2 and 2.3, respectively. The 0.1 μm-thick Au case (curves with open circles) shows a time-dependent Al foil temperature evolution similar to that of previous calculations [5] in which no Au foil was present. For Au foil thicknesses of 1 μm to 5 μm, the temperature in the Al layer increases noticeably. For instance, at 40 ns the mean temperatures in the Al layer are: $T_{Al} = 18$

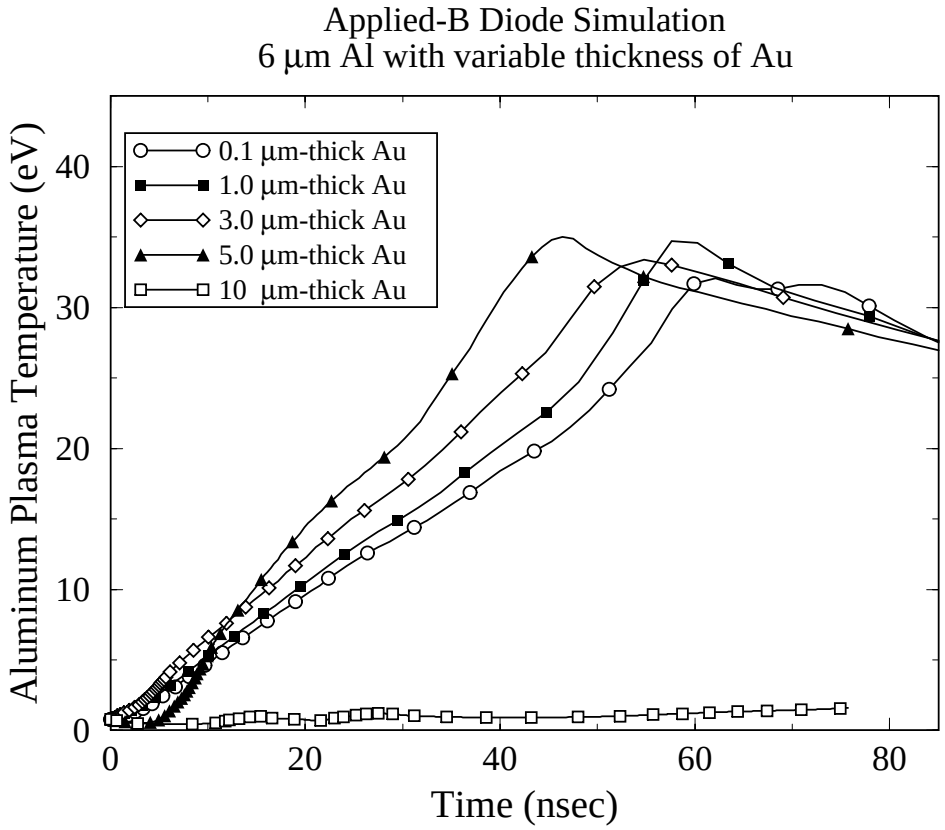

Figure 2.2. Time dependence of mean temperature in the aluminum layer for gold layer thicknesses ranging from 0.1 μm to 10 μm.

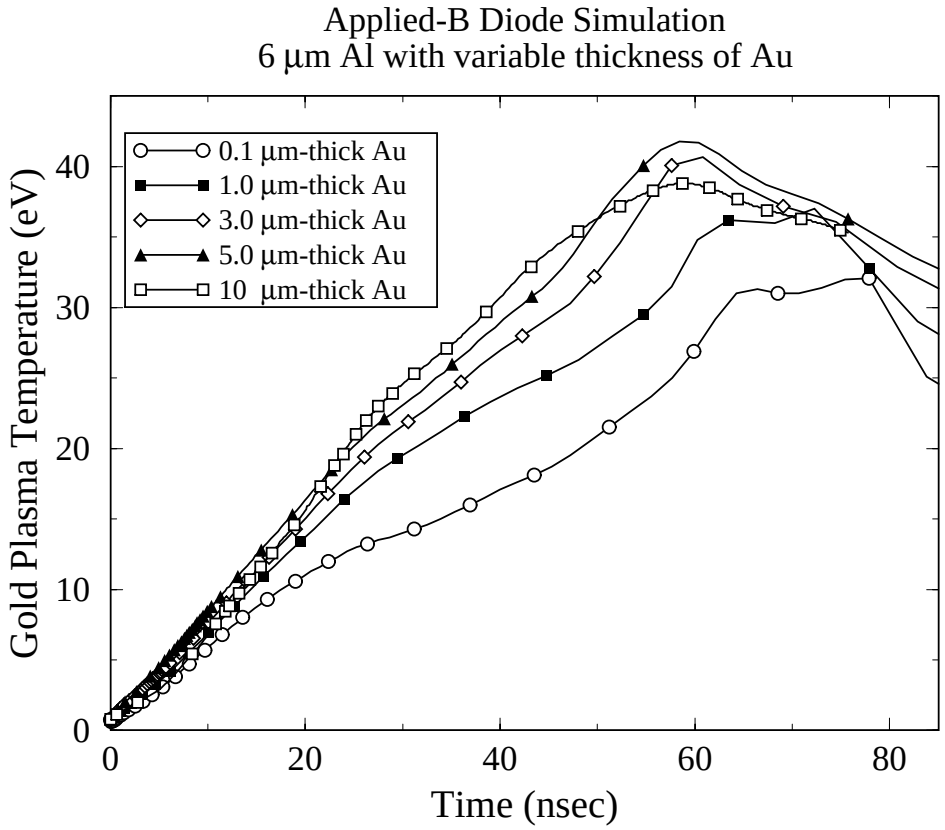

Figure 2.3. Time dependence of mean temperature in the gold layer for gold layer thicknesses ranging from 0.1 μm to 10 μm.

eV for $\Delta Ł_{Au} = 0.1$ μm, $T_{Al} = 24$ eV for $\Delta Ł_{Au} = 3$ μm, and $T_{Al} = 30$ eV for $\Delta Ł_{Au} = 5$ μm. The Al becomes hotter as the gold foil thickness increases (up to 5 μm) because the protons are slowed by the gold. The lower proton kinetic energies in the Al in turn provide for a higher stopping power (dE/dx), or energy deposition rate. Note that the temperature stops rising in the 5 μm case at about 46 ns. This occurs because the proton beam becomes unable to penetrate through the Au layer to the Al because of "range shortening" effects (that is, dE/dx increases as the temperature and ionization state of the plasma increases). It is also seen that for a 10 μm-thick Au layer, the temperature in the Al layer remains low throughout the beam pulse, while the Au temperature rises to above 35 eV. In this case, the protons do not penetrate through the Au into the Al layer.

Based on the above results, we chose to perform a complete series of radiation-hydrodynamics and CRE calculations for two-foil targets with 5 μm-thick and 0.1 μm-thick Au layers. For each case, four radiation-hydrodynamics simulations were performed (for Regions A through D). For each of the radiation-hydrodynamics simulations, a series of CRE calculations were made at simulation times ranging from 10 ns to 70 ns. In each case the CRE calculations use, as input, the radiation-hydrodynamics predictions for the depth-dependent aluminum temperature, density, proton kinetic energy, and current density. The K_α spectra from the CRE calculations are then post-processed to get time-integrated and space-integrated spectra which can be compared directly to experimental spectroscopic measurements.

Figure 2.4 shows the time-dependent mean temperatures in the Al layer for each of the four regions in the 5 μm-thick Au (solid curves) and 0.1 μm-thick Au (dashed curves) cases. In each of the regions, the Al temperatures are higher in the 5 μm Au simulations during the first $\sim$ 60 ns of the beam pulse. At later times, the beam is stopped in the Au layer prior to reaching the Al. However, previous calculations [5,6] have shown that there is little additional contribution to a time-integrated K_α emission spectrum after $\sim$ 50 ns into a KALIF beam pulse. Thus, at times when most of the K_α photons are produced, the temperatures in the Al layer can be significantly hotter ($\sim$ tens of percent) when a several-micron-thick Au foil is included.

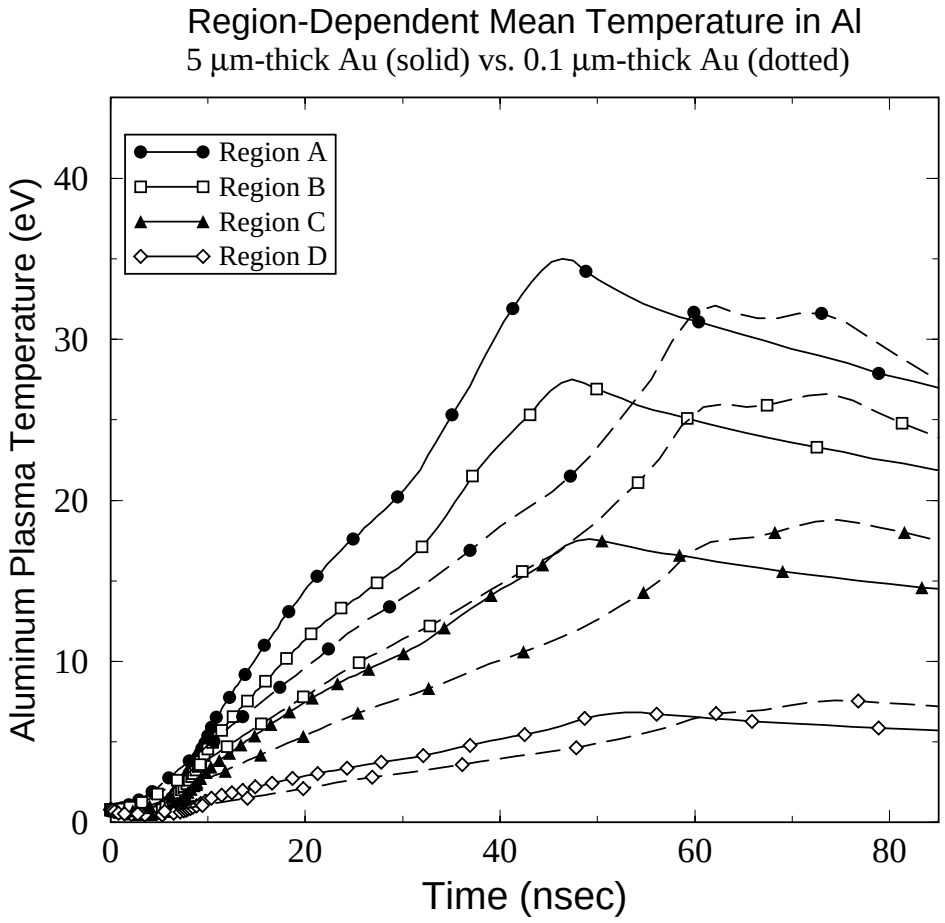

Figure 2.4. Time dependence of mean temperature in the aluminum layer for gold layer thicknesses ranging of 0.1 μm (dotted curves) and 5 μm (solid curves). Regions A through D correspond to using the beam current density parameters listed in Table 2.1.

2.3. CRE Simulations of aluminum K_α Satellite Emission and Absorption Spectra

Output from each of the 5 μm-thick and 0.1 μm-thick gold radiation-hydrodynamics simulations was used as input to NLTERT in order to predict time-dependent and time-integrated spectra. Figures 2.5 – 2.7 show aluminum K_α emission spectra for Regions A, B, and C of the 5 μm-thick Au simulations. Note the change in the flux magnitudes with time. For Region A (Fig. 2.5) it is seen that the strongest K_α emission at 40 ns comes from the Be-like and B-like Al ions. The emission from Regions B and C (and D, not shown) originates from plasma that is noticeably cooler, with emission arising from relatively low ionization stages.

Figure 2.8 shows the time-dependent Al K_α spectra for Region A of the 0.1 μm-thick Au case. Note that at 40 ns, the strongest K_α emission is due to C-like and N-like Al ions, as compared to Be-like and B-like Al in the 5 μm-thick Au case. Clearly, at a specific time and in a specific location (i.e., region) the Au layer thickness can have a very pronounced effect on the K_α satellite emission spectrum.

It is also important to note, however, that the magnitudes of the K_α line intensities are significantly lower in the 5 μm-thick Au case. For instance, at 30 ns the peak flux in the 0.1 μm case is 5×10^{12} erg/cm^2/s/eV, while it is about 0.7×10^{12} erg/cm^2/s/eV in the 5 μm case. This reduction is due to the fact that the proton-impact ionization cross section for K-shell electrons decreases as the proton energy drops. This can be more clearly seen in Figure 2.9, which shows the K_α x-ray production cross section — that is, the proton-impact ionization cross section times the fluorescence yield — as a function of the proton kinetic energy. As the proton energy drops from about 1.7 MeV to 0.6 MeV, the x-ray production cross section decreases by a factor of ~ 4. Thus, while a lower proton kinetic energy leads to a higher temperature in the Al, it also results in a lower K_α photon flux at the spectrometer.

Figures 2.10 and 2.11 show calculated time-dependent K_α absorption spectra for Region A of the 5 and 0.1 μm-thick Au simulations, respectively. Again, it is seen that at a given time, the spectra can exhibit markedly different characteristics. For expample, at $t = 40$ ns, significant absorption due to B-like Al is observed in the 5 μm Au case. By comparison, the highest Al ion showing significant absorption in the 0.1 μm Au case is N-like Al. This represents a difference of 2 full ionization stages, and should clearly show up in experiments utilizing absorption spectroscopy. Again, in a given region and at a given time, the effect of a thin gold layer ($\sim$ several microns thick) can lead to very different K_α spectral signatures.

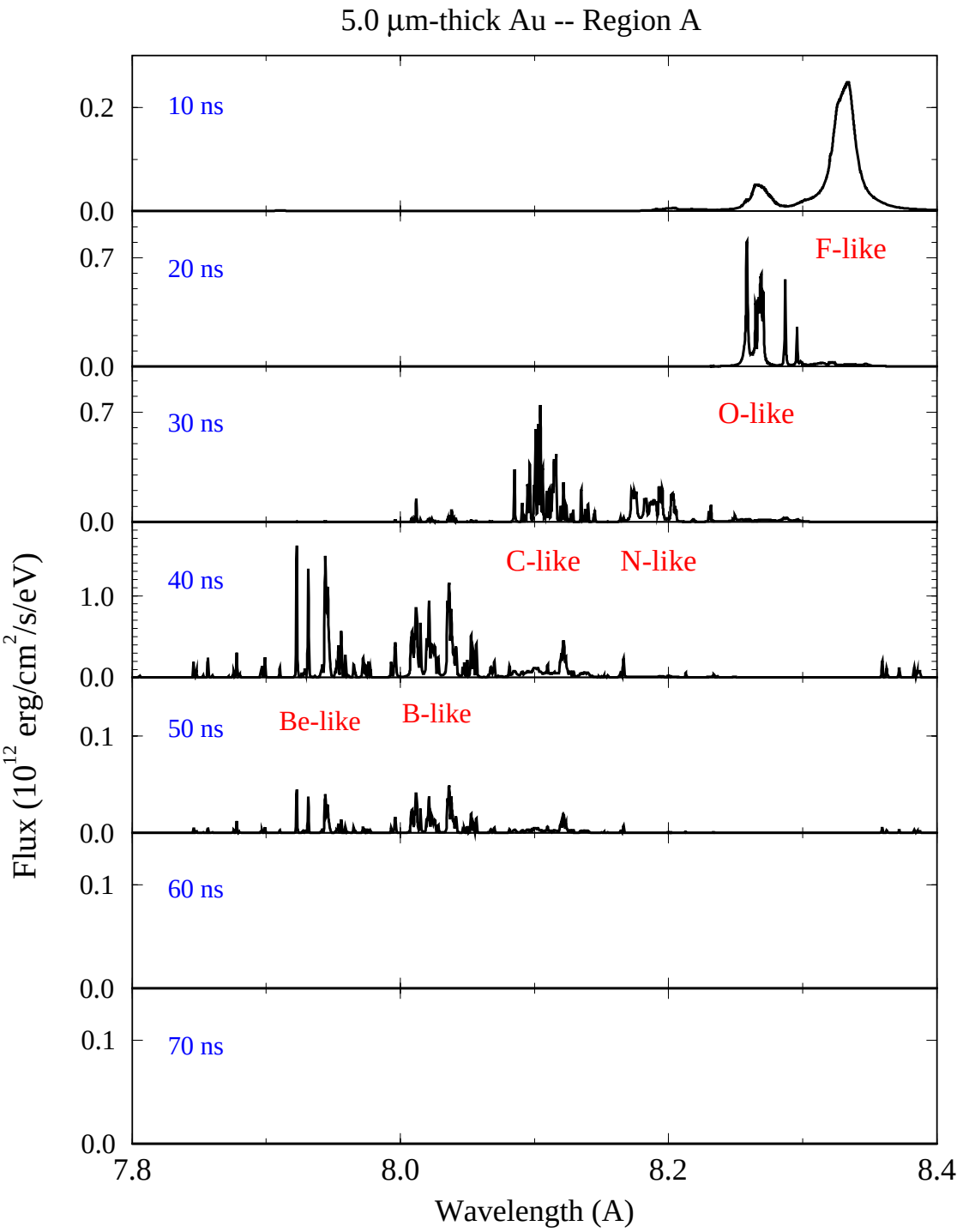

Figure 2.5. Time-dependent Al K_α emission spectra for Region A from the simulation with 5 μm Au and 6 μm Al.

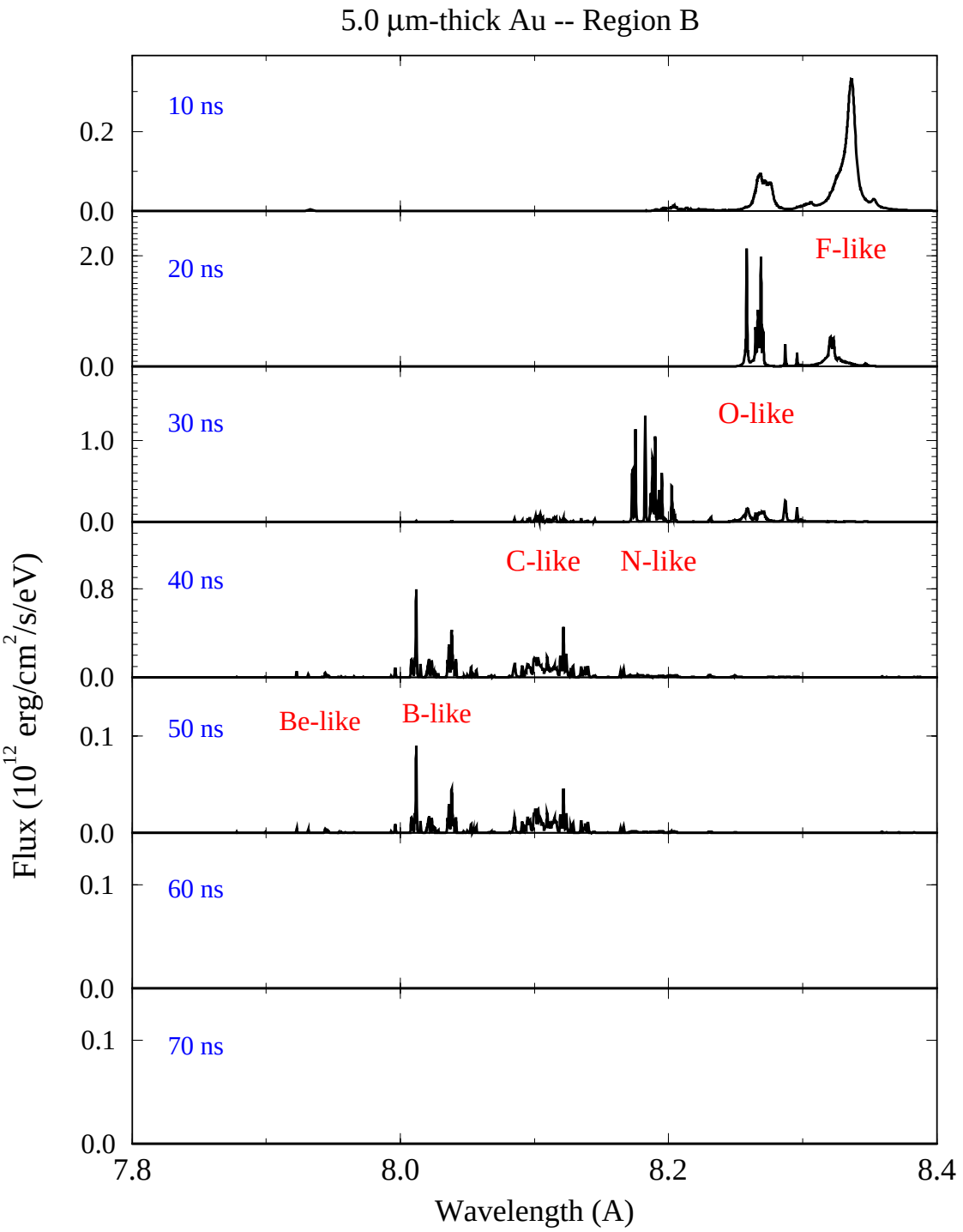

Figure 2.6. Time-dependent Al K_α emission spectra for Region B from the simulation with 5 μm Au and 6 μm Al.

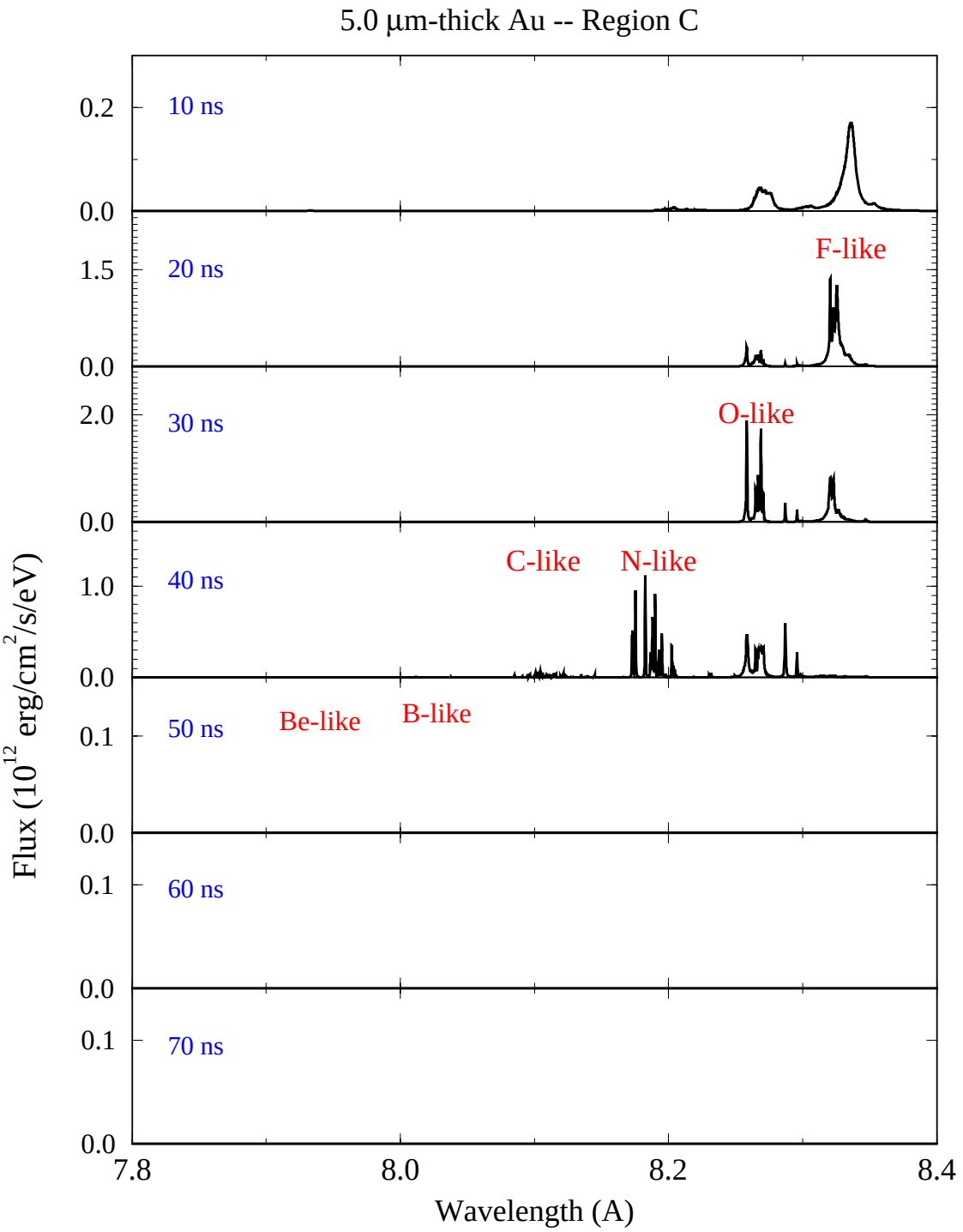

Figure 2.7. Time-dependent Al K_α emission spectra for Region C from the simulation with 5 μm Au and 6 μm Al.

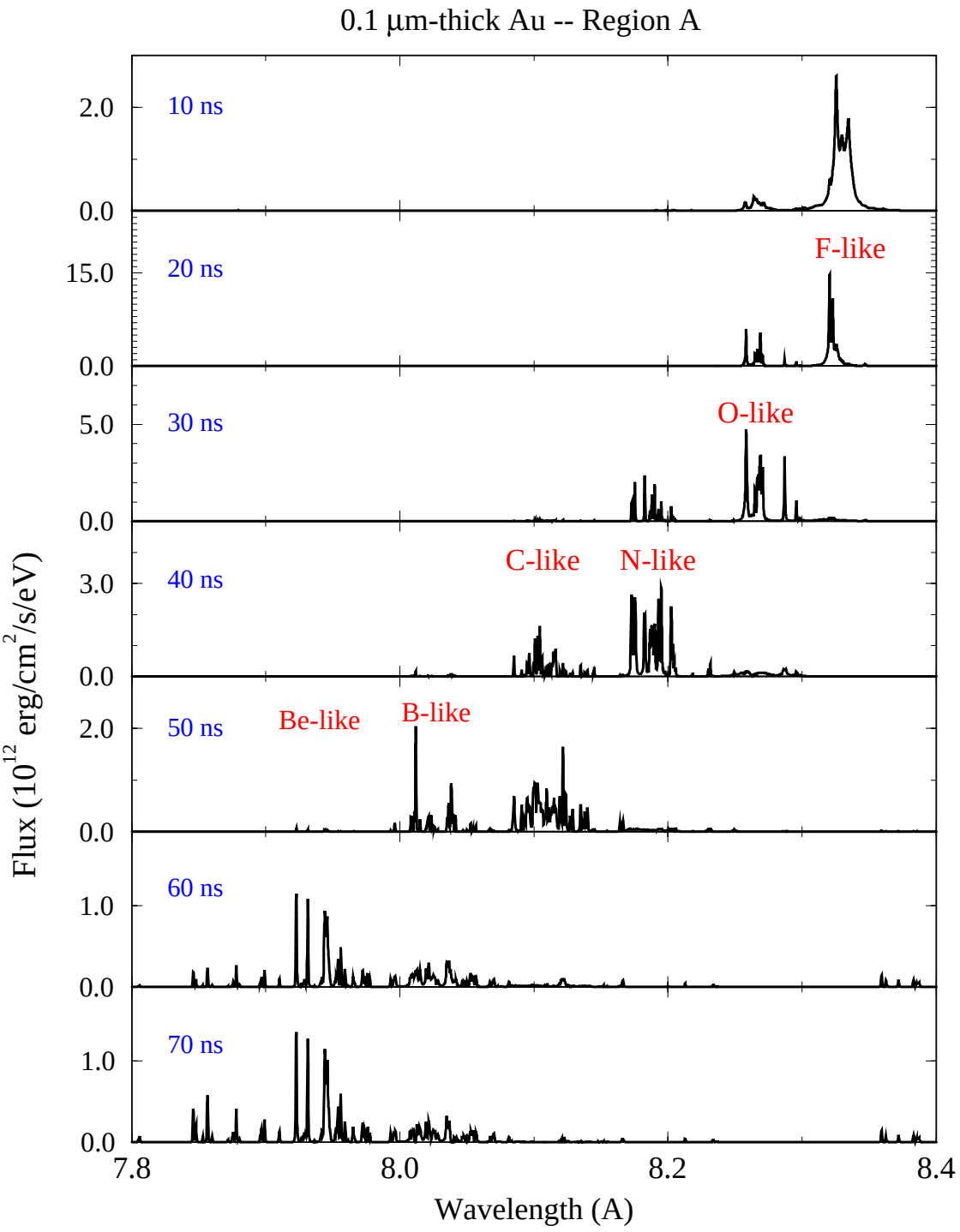

Figure 2.8. Time-dependent Al K_α emission spectra for Region A from the simulation with 0.1 μm Au and 6 μm Al.

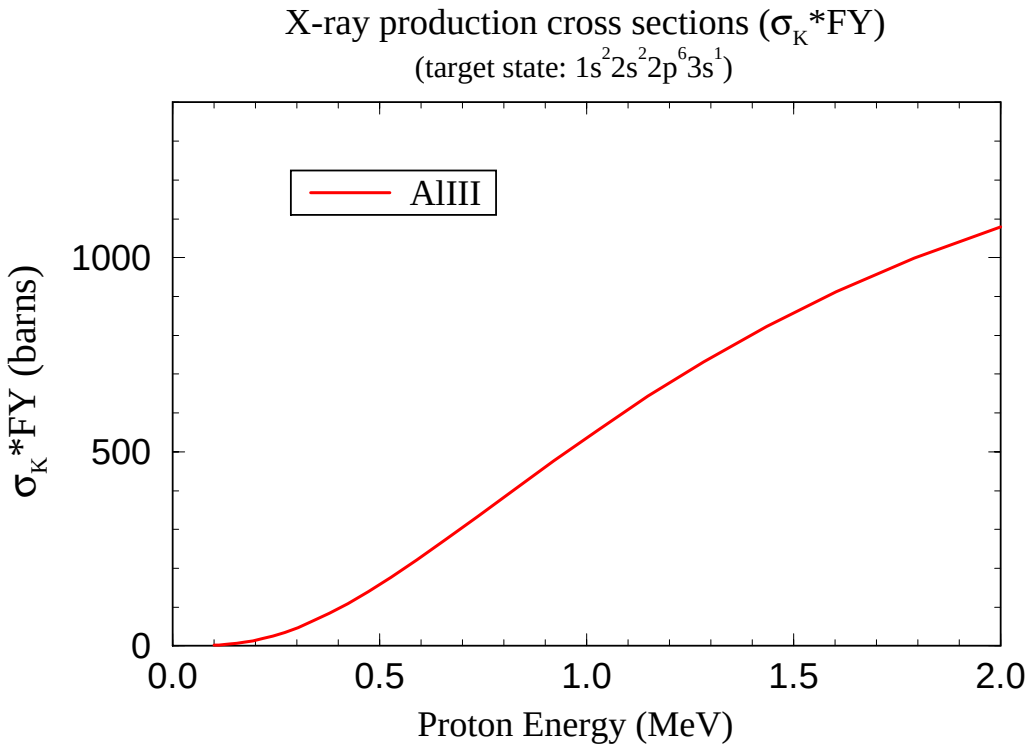

Figure 2.9. Aluminum K_α x-ray production cross section as a function of the proton beam kinetic energy.

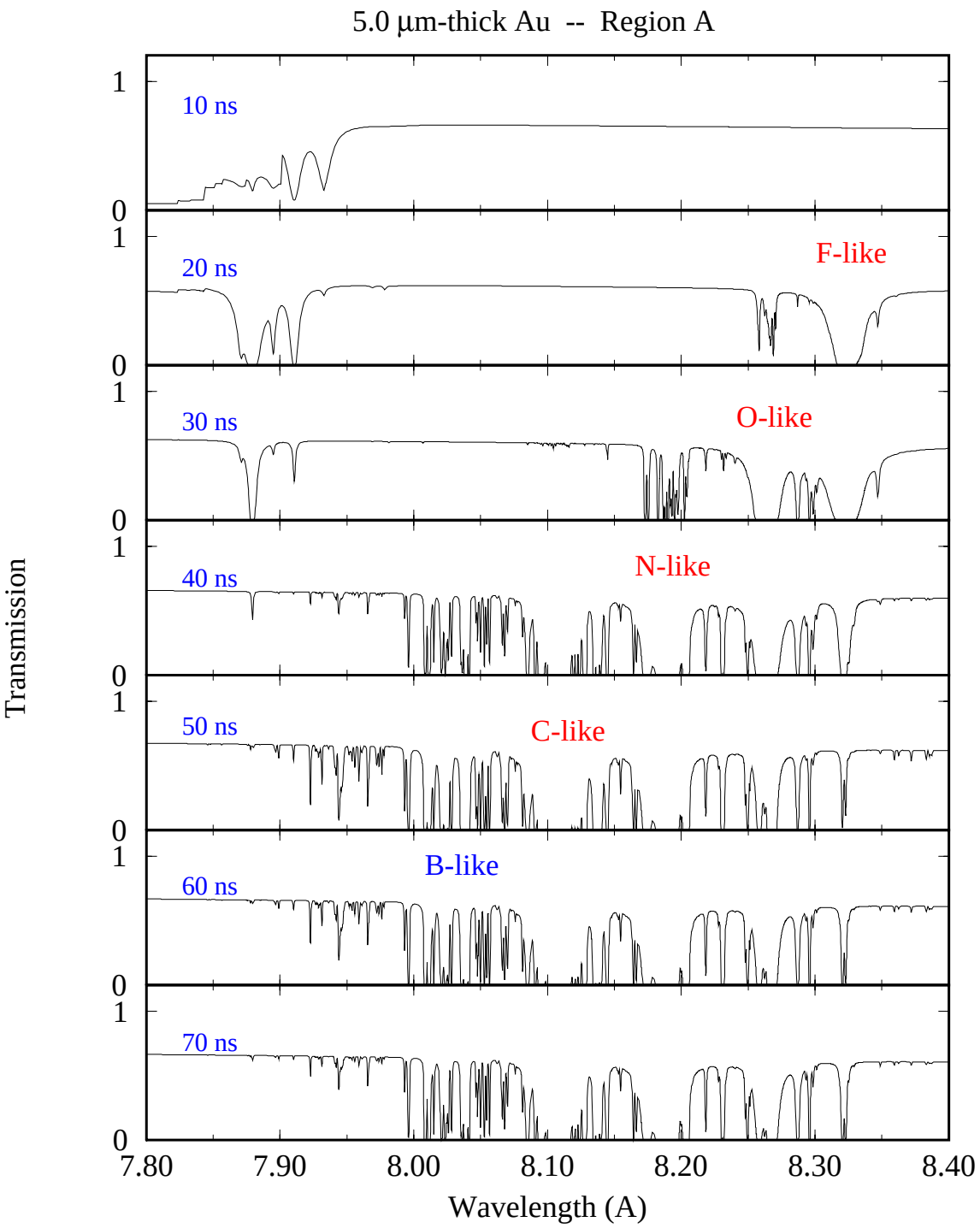

Figure 2.10. Time-dependent Al K_α absorption spectra for Region A from the simulation with 5 μm Au and 6 μm Al.

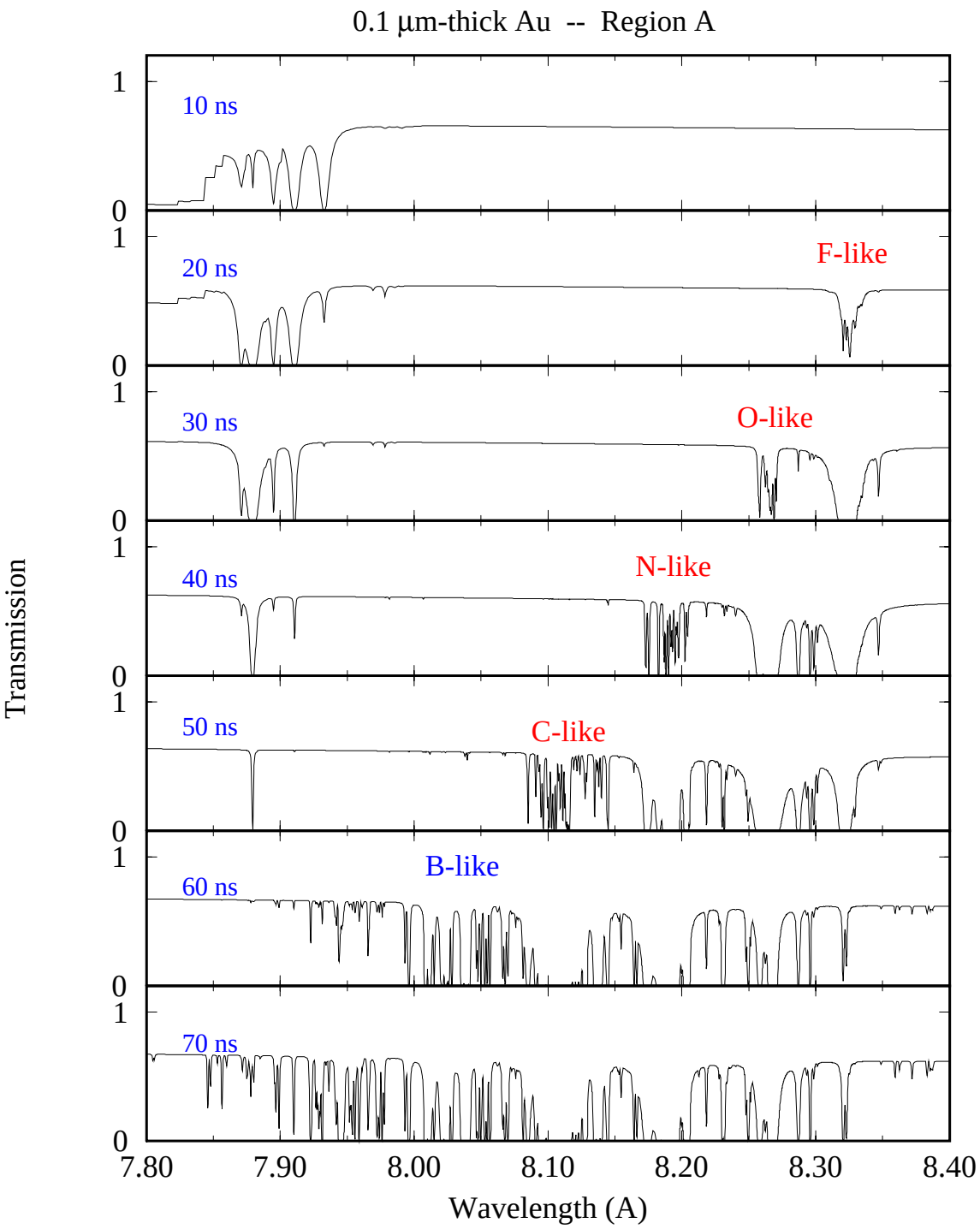

Figure 2.11. Time-dependent Al K_α absorption spectra for Region A from the simulation with 0.1 μm Au and 6 μm Al.

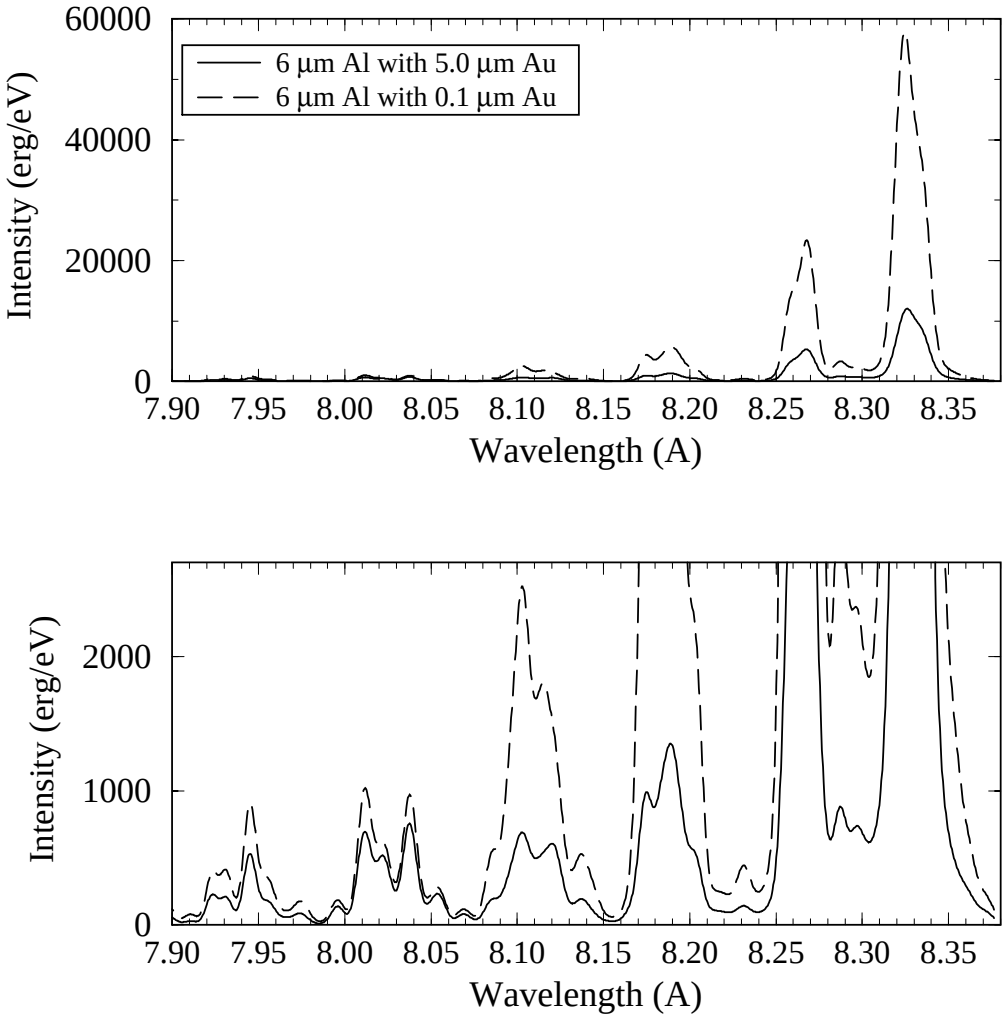

Figure 2.12. Space- and time-integrated K_α emission spectra for 5 μm Au (solid curve) and 0.1 μm Au simulations. Bottom plot shows same results on a different scale.

We next describe the effects of time-integration and space-integration on the overall spectrum. Figure 2.12 shows the synthetic time- and space-integrated spectra calculated using the areal weights given in Table 2.1. The solid and dashed curves correspond to the 5 and 0.1 μm Au cases, respectively. The lower plot in Figure 2.12 is the same data as in the upper plot, but on a different scale. The most noticeable feature in this figure is that the peak K_α fluxes for the F-like, O-like, and N-like ions (at λ = 8.33, 8.27, and 8.18 Å) are a factor of a few lower in the 5 μm Au case relative to the 0.1 μm case. This, again, results from the lower proton-impact ionization cross sections which occur as the proton kinetic energies are reduced by the gold layer. The lower plot shows that the fluxes from the Be-like and B-like ions (at λ = 7.95 and 8.04 Å, respectively) are approximately the same magnitude in the two cases. For the 5 μm case, K_α emission from Be-like Al occurs at about 40 ns into the beam pulse (see Figure 2.5), while for the 0.1 μm Au case the emission occurs at a time of $\sim$ 60 – 70 ns. The calculations predict there to be virtually no K_α emission at times $\gtrsim$ 60 ns in the 5 μm case because the ions are stopped in the Au.

The contribution to the space- and time-integrated spectra from Regions A through D are shown in Figures 2.13 and 2.14. The time-integrated spectra for Region A are represented by the bold solid curves. Note the dramatic differences in the time-integrated spectra for this relatively hot region. In the 5 μm Au simulation, the Be-like and B-like K_α satellites have intensities which are similar in magnitude to — and even somewhat greater than — those of the lower ionization stages (see lower plot in Fig. 2.13). By comparison, in the 0.1 μm Au simulation (Fig. 2.14), the fluxes from the Be-like and B-like satellites are much lower than those originating from the lower ionization states. Thus, the Au significantly influences the time-integrated spectrum emitted from the highest intensity portions of the KALIF proton beam. If the optical path to the spectrometer was apertured so that only the emission from the hottest part of the Al target were seen, one could expect to see a very pronounced difference in the overall shape of the K_α satellite spectrum as the thickness of the Au layer is changed.

2.4. Discussion

The above results predict that the characteristics of the Al K_α satellite emission spectrum can be significantly altered by positioning a thin gold layer (approximately 1 – 5 μm thick) on the beam-facing side of the Al. The presence of the Au can lead to a significantly faster rate at which the Al is heated. However, because of the lower proton

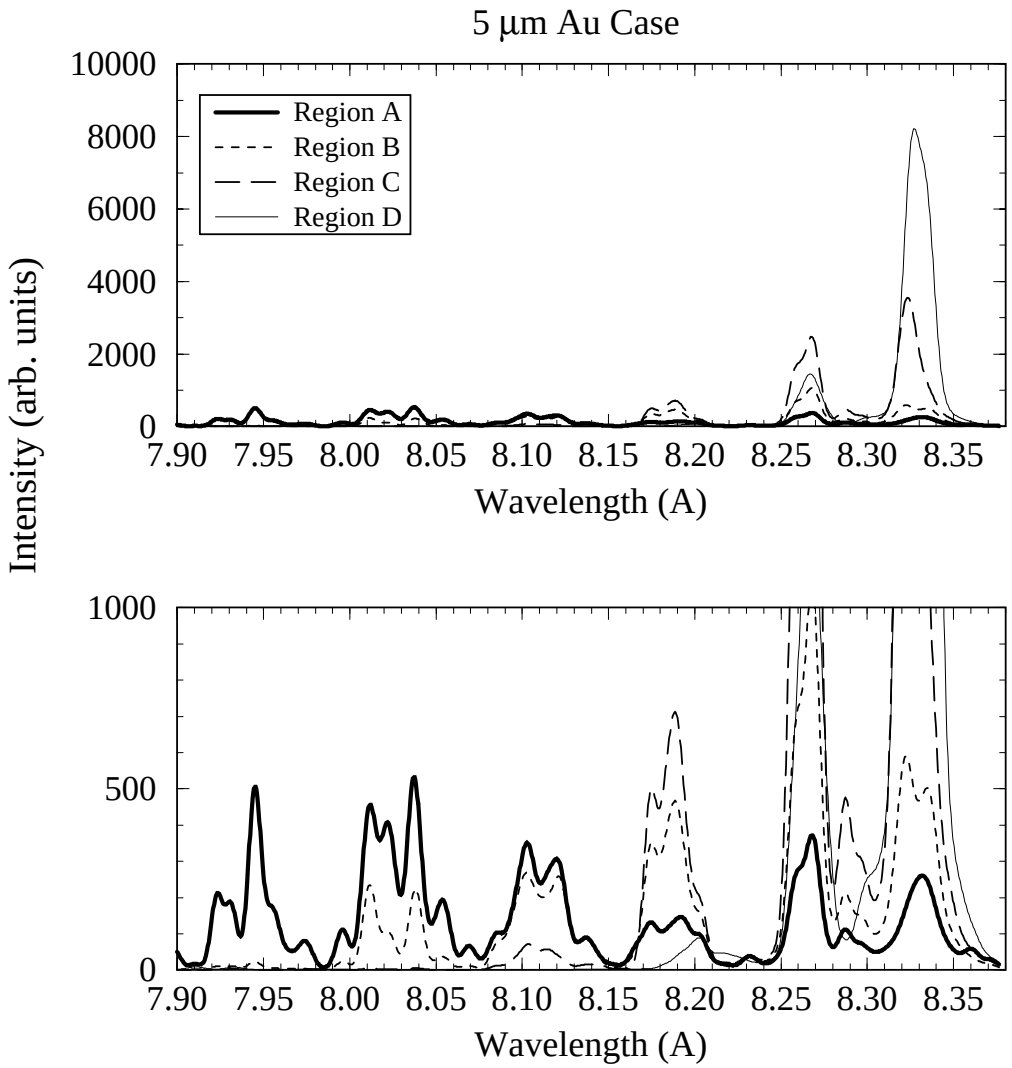

Figure 2.13. Area-weighted time-integrated Al K_α spectra from Regions A through D for 5 μm gold simulation. Bottom plot shows same results on a different scale.

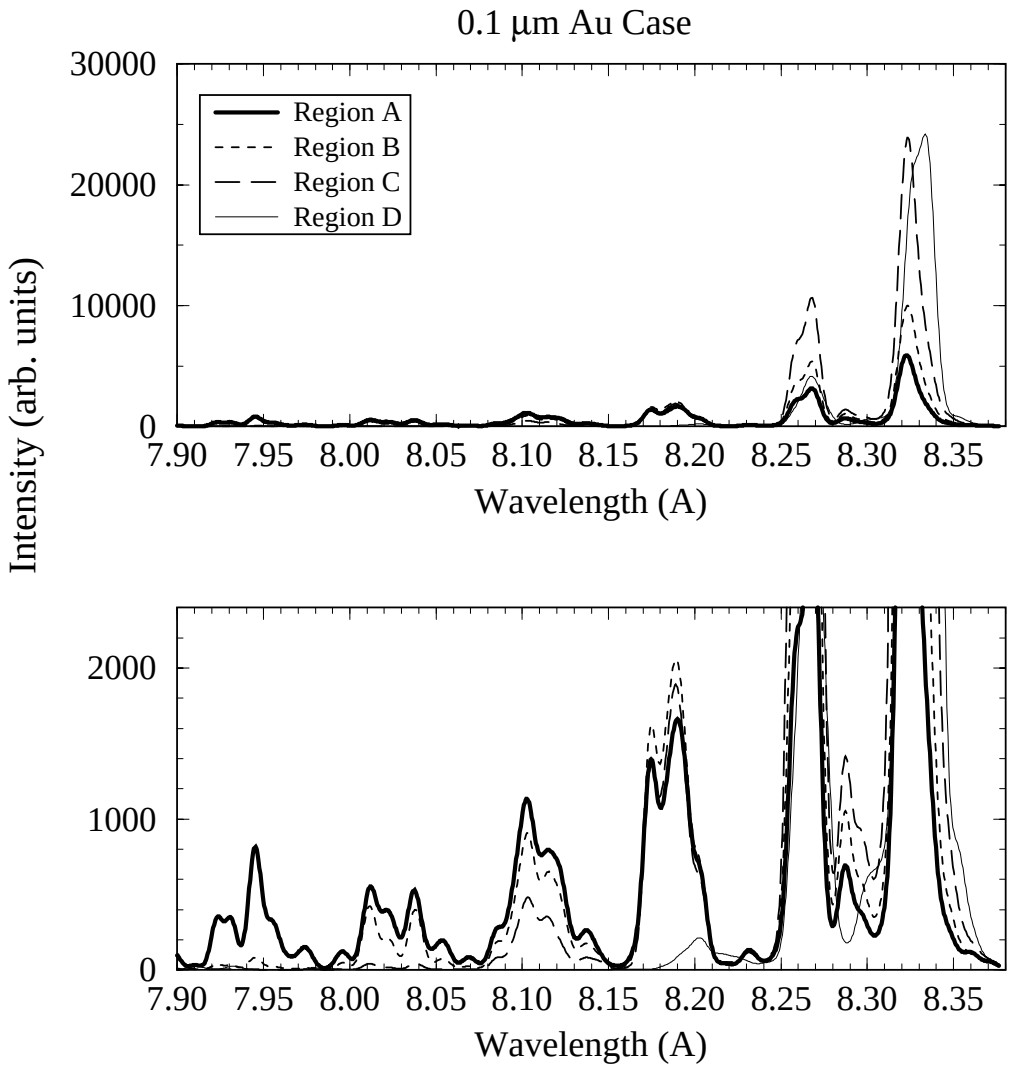

Figure 2.14. Area-weighted time-integrated Al K_α spectra from Regions A through D for 0.1 μm gold simulation. Bottom plot shows same results on a different scale.

kinetic energies in the Al the K_α line intensities can be reduced by a factor of a few. This could be a significant problem if the sensitivity of the detector is such that a reduction in the K_α photon flux means the spectrum cannot be observed. However, if the sensitivity of the detector is sufficient, it seems possible that KALIF could be used to perform a series of basic physics experiments to study the effects of an intervening gold layer (or other material) on the rate at which a second material such as Al is heated by an intense ion beam. This is particularly true if it is possible to aperture the path to the spectrometer so that emission from only a relatively small region near the center (i.e., peak) of the beam is observed, or if absorption spectroscopic measurements can be made.

Acknowledgement

Support for this work has been provided by Forschungszentrum Karlsruhe, through Fusion Power Associates.

References

1. Wang, P., "ATBASE User's Guide," Fusion Power Associates Report FPA-93-7 (December 1993).

2. J. J. MacFarlane, "NLTERT – A Collisional-Radiative Code for Computing the Radiative Properties of Non-LTE Plasmas," Fusion Power Associates Report FPA-97-2 (August 1997).

3. J. J. MacFarlane, P. Wang, J. E. Bailey, and T. A. Mehlhorn, "Diagnosing Plasma Conditions in Targets Irradiated by Intense Light Ion Beams Using K_α Satellite Line Intensity Ratios" Fusion Power Associates Report FPA-97-1 (June 1997).

4. J. J. MacFarlane, G. A. Moses, and R. R. Peterson, "BUCKY-1 – A 1-D Radiation-Hydrodynamics Code for Simulating Inertial Confinement Fusion High Energy Density Plasmas," University of Wisconsin Fusion Technology Institute Report UWFDM-984 (August 1995).

5. J. J. MacFarlane and P. Wang, "Preliminary Analysis of Aluminum K_α Satellite Spectra Obtained in KALIF Applied-B Diode Experiments," Fusion Power Associates Report FPA-96-3 (July 1996).

6. J. J. MacFarlane and P. Wang, "Collisional-Radiative, Atomic Physics, and Radiation-Hydrodynamics Simulations of Aluminum and Silicon Targets Heated by the KALIF Proton Beam," Fusion Power Associates Report FPA-96-9 (December 1996).